

# $L'$ and $M'$ standard stars for the Mauna Kea Observatories Near-Infrared (MKO–NIR) system

S.K. Leggett,<sup>1,4</sup> T.G. Hawarden,<sup>1,2</sup> M.J. Currie,<sup>1,3</sup> A.J. Adamson,<sup>1</sup> T.C. Carroll,<sup>1</sup>  
T.H. Kerr,<sup>1</sup> O.P. Kuhn,<sup>1</sup> M.S. Seigar,<sup>1</sup> W.P. Varricatt,<sup>1</sup> T. Wold<sup>1</sup>

<sup>1</sup>*Joint Astronomy Centre, University Park, Hilo, HI 96720, USA*

<sup>2</sup>*UK Astronomy Technology Centre, Royal Observatory, Blackford Hill, Edinburgh EH9 3HJ, UK*

<sup>3</sup>*Starlink Project, Rutherford Appleton Laboratory, Chilton, Didcot, Oxon OX11 0QX, UK*

<sup>4</sup>*Email: skl@jach.hawaii.edu*

30 October 2018

## ABSTRACT

We present  $L'$  and  $M'$  photometry, obtained at UKIRT using the Mauna Kea Observatories Near-IR (MKO–NIR) filter set, for 46 and 31 standard stars, respectively. The  $L'$  standards include 25 from the UKIRT in-house “Bright Standards” with magnitudes deriving from Elias et al. (1982) and observations at the IRTF in the early 1980s, and 21 fainter stars. The  $M'$  magnitudes derive from the results of Sinton & Titterton (1984). We estimate the average external error to be  $0^{\text{m}}015$  for the bright  $L'$  standards and  $0^{\text{m}}025$  for the fainter  $L'$  standards, and  $0^{\text{m}}026$  for the  $M'$  standards. The new results provide a network of homogeneously observed standards, and establish reference stars for the MKO system, in these bands. They also extend the available standards to magnitudes which should be faint enough to be accessible for observations with modern detectors on large and very large telescopes.

## 1 INTRODUCTION

Definition of an infrared photometric system was begun by Johnson and colleagues (cf. Johnson, 1966). At that time the  $L$  and  $M$  bands were rather arbitrarily defined by quite broad filters centered at around  $3.5\mu\text{m}$  and  $4.8\mu\text{m}$ . Observations at  $L$  employed as detectors

PbS cells, the long-wave sensitivity limits of which defined the edge of the band, and at  $M$  much less sensitive, broadband, bolometers or PbSe cells were used. Early infrared filters were often single remnants of manufacturers' batches and hence systems were not reproducible. In addition, early infrared filter bandpasses were not well matched to the atmospheric windows, and many absorption features, especially of water, were included. As a consequence the exact bandpass applicable to any given observation depended on the atmospheric water content, and observations were not consistent between different sites or, indeed, at the same site at different times.

The introduction of InSb detector technology made it possible to establish a new band, centred at  $3.8\mu\text{m}$  — somewhat redwards of the  $L$  band — which offered a much better match to the transmission of the terrestrial atmospheric window. This has become known as the  $L'$  band, and has effectively replaced the  $L$  band, which is no longer commonly used. An excellent review of the status of the  $LL'M$  passbands and existing systems, as it was in the late 1980s, is given by Bessell & Brett (1988).

In the mid-1980s, as infrared detector sensitivities continued to increase, many observatories found that the high thermal background admitted by the broadband  $M$  filter saturated the new detectors. Filters with narrower bandpasses were introduced; these were commonly referred to as  $M'$ . Although the same labels,  $L'$  and  $M'$ , were employed at various observatories, there were often significant differences between the particular filter bandpasses employed and hence between their resulting photometric systems.

In the late 1990s standardization of the near-infrared filter set was proposed by groups at the Gemini Observatories and the University of Hawaii (Simons & Tokunaga, 2002; Tokunaga, Simons & Vacca, 2002). This has been largely achieved by the design of bandpasses which are much less sensitive to varying water vapour conditions, and the organization of a large consortium purchase of these filters. These filters are now known as the Mauna Kea Observatories near-infrared (MKO-NIR) filter set. Note, however, that they are specifically designed to allow accurate photometry to be performed, and intercompared, at a range of altitudes, and are not simply optimised for the Mauna Kea site.

As telescope and detector technology has continued to improve, and fainter and cooler objects are discovered, observations in the thermal infrared have become ever more desirable astronomically. However, standard stars for the  $L'$  and  $M$  or  $M'$  bands are still sparse and the available set inhomogeneous. Over the last two years staff at the 3.8m UK Infrared Telescope (UKIRT) have therefore undertaken an observing programme to establish an enlarged and

homogeneous set of photometric standards, observed with improved accuracy through the MKO–NIR  $L'$  and  $M'$  filters, and extending to magnitudes faint enough to be accessible to modern (“small-well”) detectors used on 8–10-m telescopes. This paper describes that work. A history of the  $L$  and  $M$  filter bandpasses, and of the standard stars employed at UKIRT, is given in §2; the observational technique in §3; the results in §4; a discussion in §5; and our conclusions in §6.

## 2 UKIRT $L$ AND $M$ BANDPASSES AND STANDARD STARS

The list of standard stars in the  $L$ ,  $L'$  and  $M$  bandpasses used by observers at UKIRT dates from 1992 and is in-house only, having never been formally published (although at the time of writing it is available on the observatory web pages). Magnitudes were derived from Elias et al. (1982) and Sinton & Titterton (1984) supplemented by data from the *NASA Infrared Telescope Facility Photometry Manual* (1986). UKIRT observers’ own observations between 1986 and 1989 were collected in 1989 by S. Koyonagi and T. Hawarden and used to correct the  $J$ ,  $H$ ,  $K$  and  $L'$  values in the “telescope” list. A final update based on observations in 1990–91 and revised transformations to the CIT system was carried out by M.M. Casali in 1992. This list is known as the “UKIRT Bright Standards”.

From the 1990s on, use of the  $L$  and the broadband  $M$  filters ceased at UKIRT; these were replaced by  $L'$  and a narrower-band  $M'$  filter. Observers simply adopted the broad-band  $M$  magnitudes to calibrate their narrower-band  $M'$  data, since tests at the telescope had shown that there was no colour dependency between the filters, at least for spectral types earlier than K (Geballe, 1991); the presence of photospheric CO absorption was expected to lead to differences between  $M$  and  $M'$  of a few percent for later type stars. This is discussed further in §4.

UKIRT’s 1–5 $\mu$ m imager IRCAM has a 256 $\times$ 256 InSb detector array. In 1999 IRCAM was equipped with new optics, giving a smaller pixel field-of-view of 0'08. At the same time it was equipped with the MKO–NIR  $L'$  and  $M'$  filters (Simon & Tokonaga, 2002; Tokunaga et al., 2002). Figure 1 compares the previously used “UKIRT” system  $L'$  bandpass with the MKO–NIR filter, and also plots transmission profiles for the old broadband  $M$  compared with the new MKO–NIR  $M'$ .

The filter cold transmission profiles are given in Table 1, together with the profile convolved with dry and wet atmospheric conditions as shown in Figure 1. The atmospheric

transmission spectra were obtained from the Gemini Observatory web pages and were calculated by Lord (1992). The MKO–NIR filters were designed to match the atmospheric windows and to maximise throughput while providing better photometric performance. Simons & Tokunaga (2002) calculate the theoretical photometric error due to non–linear extinction to be 1.4 and 5.9 millimag for the  $L'$  and  $M'$  filters, respectively, for the Mauna Kea site. These errors increase to 3.7 and 8.1 millimag at  $L'$  and  $M'$  for a 2 km site.

To investigate the effect of changing water vapour content, we have synthesised magnitudes for the wet and dry conditions of Table 1 for G5V and M7V stars. Stellar theoretical infrared spectra were obtained from Cohen (2003, private communication) and Hauschildt, Allard & Baron (1999). These calculations showed that the effect of variable water content is small:  $\leq 3$  millimag at  $L'$  and  $\leq 5$  millimag at  $M'$ .

The filter profiles shown in Figure 1 and listed in Table 1 do not include other transmission effects due to telescope and instrument optics and the detector. The telescope mirrors are aluminised and light is reflected to the instrument from a silver–dielectric coated dichroic tertiary mirror. The camera has an uncoated calcium fluoride window and contains coated barium fluoride and uncoated lithium fluoride lenses. The detector is InSb with an anti–reflection coating. Prior to installation of the MKO–NIR filters and modification to a smaller pixel field of view, the camera had one fewer barium fluoride and lithium fluoride lens, and two additional external gold mirrors. The reflection and transmission curves of the dichroic, gold mirrors, calcium fluoride and lithium fluoride lenses are all flat within measurement error over the relevant wavelength range. The aluminised telescope mirrors have a very small change in reflectivity increasing from 98.0% at  $3\mu\text{m}$  to 98.4% at  $5\mu\text{m}$ ; the transmission of the barium fluoride lens decreases from 95.6% at  $3\mu\text{m}$  to 94.4% at  $5\mu\text{m}$ ; and the array quantum efficiency (QE) varies between 87.4% and 90.0%. Calculations of synthetic magnitudes for a G5V and an M7V star show that these optical elements effect the derived magnitudes by less than 1 millimag. To summarise, the previous UKIRT system magnitudes, and those published here, are effectively defined by the filter bandpasses and the atmospheric transmission.

We note that the newer generation InSb arrays, the  $1024\times 1024$  Aladdin arrays, have an anti–reflection coating with a more structured wavelength response. Our current thermal imager uses an Aladdin detector and also contains barium fluoride lenses whose coating has a 5%–deep feature around  $3\mu\text{m}$ . The net change to the photometric system is calculated to be  $\leq 1$  millimag except for late–type stars at  $L'$  where the difference is  $\sim 3$  millimag.

We show in §4 that the measurement errors for the primary standards presented here are typically  $0^m015$  at  $L'$  and  $0^m026$  at  $M'$ , therefore variations in the optical design of a  $3\text{--}5\mu\text{m}$  imager and telescope system are unlikely to affect the photometric system to any measurable degree. Furthermore, the MKO–NIR filters are designed to match the atmospheric windows, and appear to do so well enough that, even at a lower elevation site, the effects of variable water vapour and non–linear extinction are also substantially less than the typical observational error. Overall the results presented here using the MKO–NIR filters should be generally useable to calibrate observations with conventionally designed imagers and telescopes and on most sites.

### 3 OBSERVATIONS

IRCAM was used for all the observations, with the MKO–NIR  $L'$  and  $M'$  filters. Observations were made over 26 engineering nights (or part–nights) between 1999 September and 2002 July. Towards the end of this period, once most of the stars were well established, we used calibration data from visiting observers' runs to supplement our own measurements.

Primary standard stars were selected from the final UKIRT Bright Standards list. To avoid saturation, the stars were chosen from amongst the fainter objects on the list, with  $L' \gtrsim 7.0$  and  $M' \gtrsim 5.0$ . In addition we observed new  $L'$  secondary standards from the UKIRT (*JHK*) Faint Standards list (Hawarden et al., 2001), selecting stars that were expected to have  $L' \approx 10.0$ . Typically in a full night around 30 stars were observed, divided equally between the three groups: bright  $L'$  primary standards, faint  $L'$  secondary standards and bright  $M'$  primary standards.

The IRCAM field of view is  $20''.5$ . Observations consisted of sets of four or eight images with the telescope pointing slightly offset between each; the offsets were kept small enough that the pattern of pointings would fit inside the  $20''$  field. Consecutive pairs of images were subtracted and the set of two or four subtracted pairs were combined to give an image containing one positive and one negative detection of the source. Total exposure time for the bright  $L'$  standards was 80 seconds and for the fainter stars it was typically 480 seconds, in both cases made up of sets of four or eight 20-second exposures each in turn consisting of 100 coadded 0.2-second integrations. Exposure time at  $M'$  was usually 216 seconds, made up of sets of four or eight 9-second exposures consisting of 75 coadded 0.12-second integrations. Overheads are about a factor of two due to the extremely short integrations.

A flatfield was created by median filtering the set of four or eight normalised and cleaned observations. The cleaning removed blemishes on scales smaller than 1 arcsec, achieved by smoothing with a box filter and iteratively rejecting pixels more than two standard deviations from the neighbourhood mean. It was not necessary to mask objects when creating the flatfield because of the extremely high sky counts in every image.

The flatfielded subtracted images were registered using the telescope offsets — accurate to better than 0.5 arcsec — converted to integer numbers of pixels to avoid resampling. Mosaics of the shifted images were formed using the mean at each pixel, thus preserving flux. Counts on and off target were dominated in all cases by the high sky background and as the stars were reduced in a relative sense (described below), applying a correction for non-linearity was not necessary.

Photometry was carried out on both the positive and negative images of the source in the individual sky-subtracted and flatfielded frames as well as in the final flatfielded mosaic. The photometry aperture was automatically positioned by the software at the source centroid; the source aperture size used was  $5''.0$ . Although the background counts were close to zero, since consecutive frames had been subtracted from one another, a concentric “sky” aperture was used with inner and outer radii at  $6''.5$  and  $10''.0$ . The sky value was an iteratively clipped mean, emulating the mode.

Errors were estimated in the usual way using the variance of the pixel-to-pixel signals in the star and background apertures. The resulting error estimates were consistent with the difference in the photometry between the positive and negative image of the source, and with the scatter of the results about the observed extinction curves (see below). As a further check, for a single night’s observations, data variances were created using the read noise and Poisson statistics, and propagated through the processing steps. The photometric errors calculated using the data variance, yielded values some 20 percent larger for the mosaics than the error estimates used in this paper.

Typically two to four stars were observed repeatedly (4 to 7 times) during the night to determine the atmospheric extinction; these stars were brighter stars chosen for their location in the sky. These extinction stars were observed at airmasses as high as 2.0, typically other stars were observed at an airmass less than 1.6. The extinction was determined by a linear fit to the observed instrumental magnitude as a function of airmass. The results ranged from 0.08 to 0.15 magnitudes/airmass (hereinafter mag/AM) at  $L'$ , with an average value of 0.11 mag/AM, and ranged from 0.18 to 0.29 mag/AM at  $M'$ , with an average value of

0.23 mag/AM. The error on the extinction value was on average 0.03 mag/AM at *L'* and 0.05 mag/AM at *M'*.

Tokunaga et al. (2002) calculate the extinction for the MKO–NIR *L'* and *M'* filters; they find that a linear fit should be accurate to better than 0<sup>m</sup>005. The slope should not be strongly dependent on the amount of water in the atmosphere: for a range in precipitable water vapour of 0.5 mm to 4.0 mm the *L'* extinction should vary from 0.09 to 0.11 mag/AM and the *M'* extinction from 0.20 to 0.24 mag/AM. Our observed range of extinction values appears to be larger than predicted. However, the measurement errors are such that this difference is not significant, and we note that the means of our measured values agree with the predictions of Tokunaga et al. No significant correlation between our measured extinctions and the atmospheric water vapour content is evident.

The stars not used for extinction were observed once or twice a night. Each night's data was reduced in a relative sense: after using the extinction stars to define a mean extinction value, the primary targets were used to define a mean zeropoint at an airmass of unity. The fainter secondary standards were calibrated using these values for zeropoint and extinction. As each night's data were reduced, the deviation from the ensemble mean zeropoint for that night of the individual zeropoints from each primary standard was derived. This was applied as a correction to the catalogue magnitudes for these stars, producing an evolving working catalogue to replace the original. The evolving value was used in deriving the ensemble zeropoint, and individual deviations, on the next night, and the process repeated.

## 4 RESULTS

Table 2 gives our *L'* results for the stars from the UKIRT Bright Standards list. Spectral types for these stars were found from the SIMBAD database. The number of measurements is the number of nights on which the star was observed, i.e. if the star was observed more than once on a given night the mean result is counted as a single independent observation. Results were weighted according to the measurement error for each night. Table 3 gives the *L'* results for the fainter stars from the UKIRT Faint Standards of Hawarden et al. (2001), whence the spectral types are taken. Table 4 gives the *M'* results, where, again, the number of measurements are the number of nights observed and spectral types are from SIMBAD. For all of Tables 2 through 4, the value of  $\sigma$  given in the sixth column is the value of the standard error of the mean over all the nights included in the measurements; accordingly,

no  $\sigma$  value is shown for stars measured on only one night. This  $\sigma$  may underestimate the true external error, as we discuss below.

For the stars observed more than three times, any measurement that deviated from the mean by more than three sigma was rejected — typically these deviations were  $\approx 0^m.08$ .  $L'$  measurements were rejected for HD18881, SAO112626, HD84800, HD161903, FS104, FS123, FS125, FS147, FS149 and FS155.  $M'$  measurements were rejected for HD84800 and HD129653. In all cases single measurements were discarded, except for SAO112626 and FS155 where two  $L'$  measurements were discarded. We interpret these deviant values as simply bad data and not as evidence of variability at  $L'$  or  $M'$ . All the stars have been measured on several nights at near-infrared and, in most cases, optical wavelengths. The bright (primary) stars were observed in the  $J$ ,  $H$ ,  $K$  and  $L$  bands on numerous occasions at UKIRT (see above) and at CTIO and KPNO (Elias et al., 1982) over more than a decade. The faint stars have been observed at  $JHK$  an average of 7 (minimum: 3, maximum: 12) times over the period 1994–1998 (Hawarden et al. 2001) and in two cases are Landolt (1992) standards with numerous observations in the optical. None have been suspected to vary. Since stellar variability is usually larger in amplitude at shorter wavelengths (barring large changes in atmospheric structure, such as dust formation, unlikely in stars as carefully selected for stability and normality as these) changes of significant amplitude must be regarded as unlikely. An exception to this may be FS 101, for which the error in the mean  $L'$  value remained high despite repeat measurements. This F0 star did not show any signs of variability at  $JHK$  (Hawarden et al. 2001) but seven  $L'$  measurements showed a range of  $0^m.1$  with a standard error in the mean of  $0^m.05$ . We note that the sample includes two B supergiants, BS 696 and BS 8541, as  $M'$  standards. Although it is possible that free-free emission from potentially variable stellar winds contributes to their  $M'$  flux there is currently no evidence of variability. Sinton & Tittermore (1984) observed these stars 6–7 times and they have also been observed numerous times at UKIRT (BS 8541 is flagged as a frequently observed star in the UKIRT Bright Standards list). Note that if there is a significant contribution from a stellar wind then the stars will have atypical colours and should not be used for system transformations.

Table 5 combines all the measurements in one table, and also lists Right Ascension and Declination, proper motion and spectral type. Here we have estimated the external errors as follows. On individual nights the scatter around the mean extinction curve for stars observed more than once was typically  $0^m.02$  for the bright  $L'$  standards, and  $0^m.03$  for the fainter  $L'$



standards and for the  $M'$  standards. This is only slightly worse than the average calculated error of an individual measurement, based on signal-to-noise statistics. Accordingly, if the star was observed on  $N$  nights then our adopted uncertainty in Table 5 is the larger of  $0.02[3]/\sqrt{(N-1)}$  or the internal standard deviation of the mean given in Tables 1–3.

The number of observations in Table 5 is the number of nights on which the star was observed in each filter. A combination of lack of photometric weather and the replacement of IRCAM by another instrument necessitated the termination of this programme when some stars had fewer than three observations. These stars, and those with estimated error larger than  $0^{\text{m}}03$ , should be treated with appropriate caution, as perhaps should the two B supergiants mentioned above.

## 5 DISCUSSION

Figure 2 plots, for the brighter stars, the difference between our  $L'$  and  $M'$  magnitudes on the MKO system and the previously listed values on the UKIRT  $L'$  and broadband  $M$  systems. The differences are plotted as a function of colour, expressed as  $J - K$  on the UKIRT system (not MKO), and of brightness at  $L'$  or  $M'$ .

At  $L'$  the mean absolute difference between the current and previous measurements is  $0^{\text{m}}02$ , consistent with our uncertainties and the estimated error in the older measurements (e.g. the two stars with  $L' \approx 6$  in Sinton & Tittermore (1984) have a quoted uncertainty of  $0^{\text{m}}02$  and  $0^{\text{m}}05$  in their Table 2). There is no evidence of a colour term; instead the stars with the largest deviations from the previously tabulated value are fainter, suggesting larger errors in the original measurements. The latest spectral type in this sample is M5.5. It is known that for ultracool objects, of spectral type L5 and later, there will be a difference in magnitude measured with the previous UKIRT  $L'$  and the current MKO–NIR  $L'$  filter. This is due to the onset of methane absorption at the blue edge of the MKO–NIR bandpass (Leggett et al., 2002). Such objects are not currently used as standards.

At  $M'$  the mean absolute difference between the current and previous measurements is  $0^{\text{m}}05$ , again consistent with our estimated errors and those of the older measurements (e.g. the two stars with  $M' \approx 6$  in Sinton & Tittermore (1984) have quoted errors of  $0^{\text{m}}03$  and  $0^{\text{m}}06$ ). Again, the deviation is larger for fainter targets suggesting a larger error in the original measurement. There are insufficient red stars in common to determine whether or not a colour term exists between  $M$  and  $M'$  magnitudes. Although a dependency was expected

for types K and later due to photospheric CO absorption, we have synthesised broadband  $M$  and  $M'$  magnitudes for a late-M dwarf and for an early-K giant (using models from Hauschildt, Allard & Baron (1999) for the former and the observationally based templates of Cohen et al. (1999) for the latter) and found the difference to be only  $0^m005$ , presumably because both filters include the CO band. In any case, as broadband  $M$  is no longer used this is not an issue for modern work.

## 6 CONCLUSIONS

We have presented new  $L'$  observations, using the MKO–NIR filter, of 25 stars with  $L' \sim 7$ . The average internal standard error of the mean result for each star is  $0^m010$ , the estimated external error ranges from  $0^m010$  to  $0^m025$ . Most of these stars have previously tabulated  $L'$  values on the “UKIRT” system. The difference between the UKIRT and MKO values are typically  $0^m02$ , with one larger deviation of  $0^m09$  for the faintest star in the sample. There is no evidence of a colour dependency in  $L'_{MKO} - L'_{UKIRT}$  for stars as late as M5.5.

Data with the same filter are presented for 21 stars with  $L' \sim 10$ , taken from the UKIRT *JHK* Faint Standards list. The average internal standard error of the mean results is  $0^m02$ , the estimated external error ranges from  $0^m02$  to  $0^m05$ . These stars will be useful as standards for larger telescopes, and convenient for programs on such telescopes which require calibration of all four of the *JHKL'* bands.

We also present  $M'$  observations, using the MKO–NIR filter, of 31 stars with  $M' \sim 6.5$ . The average internal standard error of the mean results is  $0^m02$ , while the estimated external error ranges from  $0^m02$  to  $0^m05$ . Most of these stars have previously tabulated broadband  $M$  magnitudes; and the difference between  $M$  and MKO–NIR  $M'$  is typically  $0^m05$  although there are two stars that differ by  $>0^m1$ ; these are fainter stars that most likely have larger uncertainties in the original measurements. The new data will allow more accurate calibration of  $M$ –band photometry on a wide range of telescopes.

Systematic errors in the photometry due to non-linear extinction or variable water vapour are calculated to be  $\leq 4$  millimag at  $L'$  and  $\leq 8$  millimag at  $M'$ , for sites as low as 2 km. Investigation of the transmissive or reflective elements of UKIRT and its imagers implies that commonly used optical elements will introduce variations in the photometric system of  $\leq 3$  millimag. Hence the results presented here are generally applicable to other observatories.

**ACKNOWLEDGMENTS**

UKIRT, the United Kingdom Infrared Telescope, is operated by the Joint Astronomy Centre on behalf of the U.K. Particle Physics and Astronomy Research Council (PPARC). This work would not have been possible without the dedicated effort of all the UKIRT staff, past and present; in particular we note the important contribution of the late Sidney Arakaki, without which none of the early UKIRT photometry would have been possible. We are very grateful to Mark Casali, Tim Chuter, Maren Hauschildt–Purves, Kevin Krisciunas, Andy Longmore, Erik Starman, Mike Wagner and Peredur Williams, as well as vacation student Stuart K. Koyonagi. We thank visiting observers Dave Golimowski and Gene Magnier for allowing us to incorporate their calibration observations in these results. We also thank the referee for a careful reading of the manuscript and for suggestions that lead to substantial improvements.

ORAC–DR was used to reduce the observations for this paper. ORAC–DR was developed at the Joint Astronomy Centre; the concept and early recipes originated at the Astronomy Technology Centre, Edinburgh. The application engines used in ORAC–DR were supplied and excellently supported by the Starlink Project, which is run by the UK Central Laboratory for the Research Councils on behalf of PPARC. We thank all the programmers involved.

**REFERENCES**

- Bessell M.S & Brett J.M., 1988, *PASP*, 100, 1134
- Cohen M., Walker, R.G., Carter, B., Hammersley, P., Kidger, M. & Noguchi, K., 1999, *AJ*, 117, 1864
- Elias J.H., Frogel J.A., Matthews K. & Neugebauer G., 1982, *AJ*, 87, 1029
- Geballe T.R., 1991, *The JCMT-UKIRT Newsletter*, 2, 6
- Hauschildt P.H., Allard, F. & Baron, E., 1999, *ApJ*, 512, 377
- Hawarden T.G., Leggett S.K., Letawsky M.B., Ballantyne D.R. & Casali M.M., 2001, *MNRAS*, 325, 563.
- Johnson H.L., 1966, *ARA&A*, 4, 193
- Landolt A.U., 1992, *AJ*, 104, 340
- Leggett S.K. et al. 2002, *ApJ*, 564, 452
- Lord S.D., 1992, *NASA Technical Memor.* 103957
- Simons D.A. & Tokunaga A.T., 2002, *PASP*, 114, 169

Sinton W.M. & Tittlemore W.C., 1984, AJ, 89, 1366

Tokunaga A.T., Simons D.A. & Vacca W.D., 2002, PASP, 114, 180

**Table 1.** Profiles of the MKO–NIR *L'* and *M'* filters at cold temperatures, and including the effect of absorption by an atmosphere with 1.2 mm and 3 mm of water vapour.

<i>L'</i>		H <sub>2</sub> O		<i>M'</i>		H <sub>2</sub> O	
Wavelength $\mu\text{m}$	Transmission %	1.2mm	3.0mm	Wavelength $\mu\text{m}$	Transmission %	1.2mm	3.0mm
3.22	0.0	0.0	0.0	4.38	0.0	0.0	0.0
3.24	0.1	0.1	0.1	4.40	0.2	0.0	0.0
3.26	0.1	0.1	0.1	4.42	0.2	0.0	0.0
3.28	0.2	0.2	0.1	4.44	0.5	0.0	0.0
3.30	0.6	0.4	0.3	4.46	0.3	0.0	0.0
3.32	1.1	0.5	0.4	4.48	0.3	0.1	0.0
3.34	1.9	1.5	1.3	4.50	0.7	0.3	0.3
3.36	3.1	2.4	2.1	4.52	2.0	0.6	0.6
3.38	6.1	4.6	4.2	4.54	8.6	3.6	3.3
3.40	16.2	12.2	11.6	4.56	36.8	21.3	20.0
3.42	43.2	37.1	36.5	4.58	84.4	58.6	54.6
3.44	76.7	74.1	72.1	4.60	91.3	73.8	70.2
3.46	90.1	85.9	83.1	4.62	92.0	78.3	75.5
3.48	91.8	87.9	86.1	4.64	93.2	80.0	77.0
3.50	91.6	89.5	87.6	4.66	91.5	80.2	73.2
3.52	89.4	87.8	85.8	4.68	89.4	73.8	65.2
3.54	87.6	80.9	78.6	4.70	88.8	66.8	66.2
3.56	87.9	84.0	81.7	4.72	89.6	64.7	62.9
3.58	89.6	84.4	81.4	4.74	90.8	72.1	70.2
3.60	91.4	87.8	85.4	4.76	89.1	69.3	67.2
3.62	92.7	89.6	87.5	4.78	78.0	59.4	52.4
3.64	93.6	90.6	89.0	4.80	53.9	44.1	40.0
3.66	94.1	91.5	90.0	4.82	25.6	19.6	17.4
3.68	93.6	89.3	84.5	4.84	9.1	5.4	4.4
3.70	92.8	90.3	89.1	4.86	3.0	2.4	2.3
3.72	91.5	88.3	86.8	4.88	1.1	1.0	1.0
3.74	90.6	86.9	85.8	4.90	0.5	0.4	0.2
3.76	91.0	86.7	84.4	4.92	0.5	0.5	0.5
3.78	91.7	88.1	86.2	4.94	0.0	0.0	0.0
3.80	92.1	87.7	86.2				
3.82	92.7	88.4	86.6				
3.84	92.8	87.4	85.5				
3.86	92.7	86.0	84.2				
3.88	93.1	80.4	78.1				
3.90	93.6	84.2	82.5				
3.92	94.1	81.9	79.8				
3.94	93.7	83.3	81.8				
3.96	92.5	83.3	82.0				
3.98	90.8	80.4	79.2				
4.00	89.7	77.7	76.3				
4.02	90.2	75.6	74.0				
4.04	91.7	73.2	71.4				
4.06	93.7	72.6	70.6				
4.08	92.2	67.5	65.2				
4.10	79.3	54.4	52.3				
4.12	53.3	30.5	29.0				
4.14	27.2	10.5	9.9				
4.16	10.6	2.5	2.3				
4.18	4.2	0.3	0.3				
4.20	1.9	0.1	0.0				
4.22	0.8	0.0	0.0				
4.24	0.4	0.0	0.0				
4.26	0.0	0.0	0.0				

**Table 2.** New  $L'$  Photometry for Bright Standards

Name	Other Names	RA/Dec equinox 2000	Spectral Type	$L'$ mag	$\sigma$ mag	Number of Observations
HD225023	SAO53596	00:02:46.03 +35:48:55.7	A0	6.979	0.001	3
G158-27	GJ1002	00:06:43.00 -07:32:42.0	M5.5V	6.989	0.018	4
HD1160	SAO109094	00:15:57.30 +04:15:04.0	A0	7.055	0.005	3
HD3029	SAO74098	00:33:39.53 +20:26:01.7	A3	7.082	0.014	4
HD18881	SAO56114	03:03:31.94 +38:24:36.1	A0	7.160	0.007	3
HD22686	SAO111318	03:38:55.09 +02:45:48.6	A0	7.199	0.008	4
SAO112626	HD287736	05:19:17.16 +01:42:16.1	G0	8.559	0.010	3
HD38921	SAO196174	05:47:22.19 -38:13:51.3	A0V	7.513	0.013	2
HD40335	SAO113311	05:58:13.52 +01:51:23.0	A0	6.441	0.025	2
HD44612	SAO41080	06:24:46.60 +43:32:54.5	A0	7.050	0.002	3
HD77281	SAO136505	09:01:38.01 -01:28:34.8	A2	7.041	0.014	6
GL347A	G161-33	09:28:53.50 -07:22:15.0	M2.5V	7.367	0.009	3
HD84800	SAO43050	09:48:44.64 +43:39:55.6	A2II	7.547	0.013	5
HD105601	SAO62866	12:09:27.80 +38:37:54.6	Am	6.669	0.011	3
HD106965	SAO119313	12:17:57.54 +01:34:31.1	A2	7.311	0.010	6
HD129653	SAO64289	14:42:39.56 +36:45:24.3	A2	6.920	0.007	3
HD129655	SAO140097	14:43:46.44 -02:30:20.0	A2	6.666	0.014	3
HD136754	SAO83785	15:21:34.53 +24:20:36.1	A0	7.158	0.010	5
HD162208	SAO66344	17:47:58.56 +39:58:50.9	A0	7.125	0.011	3
HD161903	SAO141886	17:48:19.22 -01:48:29.7	A2	7.034	0.005	3
HD161743	SAO209292	17:48:57.93 -38:07:07.5	B9IV	7.623	0.001	2
GL748	G22-18	19:12:14.60 +02:53:11.1	M3.5V	6.012	0.017	2
GL811.1	Wolf 896	20:56:46.60 -10:26:54.6	M2.5V	6.691	0.006	3
HD203856	SAO71278	21:23:35.53 +40:01:07.0	A0	6.871	0.013	5
SAO34401	HD212533	22:23:42.24 +55:12:25.1	F0V	7.735	0.013	6

**Table 3.** New  $L'$  Photometry for Faint Standards

UKIRT FS Number	Other Names	RA/Dec equinox 2000	Spectral Type	$L'$ mag	$\sigma$ mag	Number of Observations
101	CMC400101	00:13:43.58 +30:37:59.9	F0	10.34	0.05	7
2	SA92-342	00:55:09.93 +00:43:13.1	F5	10.44	0.02	4
104	P194-R	01:04:59.43 +41:06:30.8	A7	10.36	0.03	3
107	CMC600954	01:54:10.14 +45:50:38.0	G0	10.18	0.02	3
108	CMC502032	03:01:09.85 +46:58:47.7	F8	9.65	0.01	3
109	LHS169	03:13:24.16 +18:49:38.4	M2V	10.50	0.01	3
111	CMC601790	03:41:08.55 +33:09:35.5	G5	10.23	0.01	3
117	B216-b9	04:23:56.61 +26:36:38.0	N/A	9.75	0.01	2
119	SAO131719	05:02:57.44 -01:46:42.6	A2	9.80	0.01	2
13	SA97-249	05:57:07.59 +00:01:11.4	G4	10.10	0.03	2
123	P486-R	08:51:11.88 +11:45:21.5	B8	10.25	0.02	4
125	P259-C	09:03:20.60 +34:21:03.9	G8	10.33	0.03	3
129	LHS2397a	11:21:48.95 -13:13:07.9	M8V	10.03	N/A	1
134	LHS2924	14:28:43.37 +33:10:41.5	M9V	10.10	0.02	3
138	P275-A	16:28:06.72 +34:58:48.3	A1	10.44	0.03	3
140	S587-T	17:13:22.65 -18:53:33.8	G9	10.34	0.01	2
147	P230-A	19:01:55.27 +42:29:19.6	A0	9.84	0.02	3
148	S810-A	19:41:23.52 -03:50:56.1	A0	9.46	0.02	4
149	P338-C	20:00:39.25 +29:58:40.0	B7.5	10.06	0.02	5
150	CMC513807	20:36:08.44 +49:38:23.5	G0	9.91	0.02	4
155	CMC516589	23:49:47.82 +34:13:05.1	K5	9.32	0.02	5

**Table 4.** New *M'* Photometry for Standards

Name	Other Names	RA/Dec equinox 2000	Spectral Type	<i>M'</i> mag	$\sigma$ mag	Number of Observations
HD225023	SAO53596	00:02:46.03 +35:48:55.7	A0	6.95	0.03	8
G158-27	GJ1002	00:06:43.00 -07:32:42.0	M5.5V	7.03	0.05	2
HD1160	SAO109094	00:15:57.30 +04:15:04.0	A0	7.04	0.01	3
HD3029	SAO74098	00:33:39.53 +20:26:01.7	A3	7.04	0.02	3
BS696	HD14818	02:25:16.03 +56:36:35.4	B2Iae	5.32	0.03	3
HD18881	SAO56114	03:03:31.94 +38:24:36.1	A0	7.17	0.02	3
HD22686	SAO111318	03:38:55.09 +02:45:48.6	A0	7.16	0.02	4
BS1140	HD23288	03:44:48.22 +24:17:22.1	B7IV	5.57	0.02	3
BS1869	HD36719	05:36:15.96 +47:42:55.0	F0V	5.40	N/A	1
HD38921	SAO196174	05:47:22.19 -38:13:51.3	A0V	7.49	0.02	2
HD40335	SAO113311	05:58:13.52 +01:51:23.0	A0	6.41	0.01	5
BS2228	HD43244	06:17:34.65 +46:25:26.2	F0V	5.87	0.02	2
HD44612	SAO41080	06:24:46.60 +43:32:54.5	A0	7.07	0.03	3
HD77281	SAO136505	09:01:38.01 -01:28:34.8	A2	7.02	0.03	5
HD84800	SAO43050	09:48:44.64 +43:39:55.6	A2II	7.56	0.01	5
HD105601	SAO62866	12:09:27.80 +38:37:54.6	Am	6.70	0.02	3
HD106965	SAO119313	12:17:57.54 +01:34:31.1	A2	7.32	0.04	3
HD129653	SAO64289	14:42:39.56 +36:45:24.3	A2	6.99	0.01	3
HD129655	SAO140097	14:43:46.44 -02:30:20.0	A2	6.69	0.02	3
HD136754	SAO83785	15:21:34.53 +24:20:36.1	A0	7.13	0.04	4
BS6092	HD147394	16:19:44.44 +46:18:48.1	B5IV	4.37	0.01	2
HD162208	SAO66344	17:47:58.56 +39:58:50.9	A0	7.05	0.02	3
HD161903	SAO141886	17:48:19.22 -01:48:29.7	A2	6.97	0.01	3
HD161743	SAO209292	17:48:57.93 -38:07:07.5	B9IV	7.67	N/A	1
GL748	G22-18	19:12:14.60 +02:53:11.1	M3.5V	6.00	0.01	2
BS7773	HD193432	20:20:39.82 -12:45:32.7	B9IV	4.86	0.02	3
GL811.1	Wolf 896	20:56:46.60 -10:26:54.6	M2.5V	6.72	0.02	3
HD201941	SAO126618	21:12:45.32 +02:38:33.9	A2	6.63	0.03	3
HD203856	SAO71278	21:23:35.53 +40:01:07.0	A0	6.84	0.01	3
SAO34401	HD212533	22:23:42.24 +55:12:25.1	F0V	7.70	0.02	3
BS8541	HD212593	22:24:30.99 +49:28:35.0	B9Iab	4.20	0.01	3

**Table 5.** Summary of  $L'$   $M'$  Photometry

Name	Other Name	RA/Dec equinox 2000	Proper Motion mas/year	Type	$L'$ mag	Estimated Error	$M'$ mag	Estimated Error	Number of Obs.
HD225023	SAO53596	00:02:46.03 +35:48:55.7	+14 -2	A0	6.979	0.014	6.95	0.03	3,8
G158-27	GJ1002	00:06:43.00 -07:32:42.0	-623 -2037	M5.5V	6.989	0.018	7.03	0.05	4,2
FS101	CMC400101	00:13:43.58 +30:37:59.9	-5 -9	F0	10.34	0.05			7,0
HD1160	SAO109094	00:15:57.30 +04:15:04.0	+21 -14	A0	7.055	0.014	7.04	0.02	3,3
HD3029	SAO74098	00:33:39.53 +20:26:01.7	+4 +1	A3	7.082	0.014	7.04	0.02	4,3
FS2	SA92-342	00:55:09.93 +00:43:13.1		F5	10.44	0.02			4,0
FS104	P194-R	01:04:59.43 +41:06:30.8	+0 -4	A7	10.36	0.03			3,0
FS107	CMC600954	01:54:10.14 +45:50:38.0	-25 -4	G0	10.18	0.02			3,0
BS696	HD14818	02:25:16.03 +56:36:35.4	-0 -1	B2Iae			5.32	0.03	0,3
FS108	CMC502032	03:01:09.85 +46:58:47.7	+1 -1	F8	9.65	0.02			3,0
HD18881	SAO56114	03:03:31.94 +38:24:36.1	+5 -12	A0	7.160	0.014	7.17	0.02	3,3
FS109	LHS169	03:13:24.16 +18:49:38.4	+1346 -1103	M2V	10.50	0.02			3,0
HD22686	SAO111318	03:38:55.09 +02:45:48.6	+24 -20	A0	7.199	0.012	7.16	0.02	4,4
FS111	CMC601790	03:41:08.55 +33:09:35.5	+3 +3	G5	10.23	0.02			3,0
BS1140	HD23288	03:44:48.22 +24:17:22.1	+21 -44	B7IV			5.57	0.02	0,3
FS117	B216-b9	04:23:56.61 +26:36:38.0		N/A	9.75	0.03			2,0
FS119	SAO131719	05:02:57.44 -01:46:42.6	+1 -6	A2	9.80	0.03			2,0
SAO112626	HD287736	05:19:17.16 +01:42:16.1	+22 -41	G0	8.559	0.010			3,0
BS1869	HD36719	05:36:15.96 +47:42:55.0	+14 -20	F0V			5.40	0.03	0,1
HD38921	SAO196174	05:47:22.19 -38:13:51.3	+0 -7	A0V	7.513	0.020	7.49	0.03	2,2
FS13	SA97-249	05:57:07.59 +00:01:11.4		G4	10.10	0.03			2,0
HD40335	SAO113311	05:58:13.52 +01:51:23.0	+6 -7	A0	6.441	0.025	6.41	0.02	2,5
BS2228	HD43244	06:17:34.65 +46:25:26.2	-44 +11	F0V			5.87	0.03	0,2
HD44612	SAO41080	06:24:46.60 +43:32:54.5	+0 -22	A0	7.050	0.014	7.07	0.03	3,3
FS123	P486-R	08:51:11.88 +11:45:21.5	-8 -6	B8	10.25	0.02			4,0
HD77281	SAO136505	09:01:38.01 -01:28:34.8	-16 -13	A2	7.041	0.014	7.02	0.03	5,5
FS125	P259-C	09:03:20.60 +34:21:03.9		G8	10.33	0.03			3,0
GL347A	G161-33	09:28:53.50 -07:22:15.0	-165 -672	M2.5V	7.367	0.014			3,0
HD84800	SAO43050	09:48:44.64 +43:39:55.6	-28 -30	A2II	7.547	0.013	7.56	0.02	5,5
FS129	LHS2397a	11:21:48.95 -13:13:07.9	-399 -348	M8V	10.03	0.03			1,0
HD105601	SAO62866	12:09:27.80 +38:37:54.6	-33 -60	Am	6.669	0.014	6.70	0.02	3,3
HD106965	SAO119313	12:17:57.54 +01:34:31.1	-26 -7	A2	7.311	0.010	7.32	0.04	6,3
FS134	LHS2924	14:28:43.37 +33:10:41.5	-337 -747	M9V	10.10	0.02			3,0
HD129653	SAO64289	14:42:39.56 +36:45:24.3	+29 -10	A2	6.920	0.014	6.99	0.02	3,3
HD129655	SAO140097	14:43:46.44 -02:30:20.0	-31 -26	A2	6.666	0.014	6.69	0.02	3,3
HD136754	SAO83785	15:21:34.53 +24:20:36.1	-36 -9	A0	7.158	0.010	7.13	0.04	5,4
BS6092	HD147394	16:19:44.44 +46:18:48.1	-13 +39	B5IV			4.37	0.03	0,2
FS138	P275-A	16:28:06.72 +34:58:48.3	-12 +5	A1	10.44	0.03			3,0
FS140	S587-T	17:13:22.65 -18:53:33.8		G9	10.34	0.03			2,0
HD162208	SAO66344	17:47:58.56 +39:58:50.9	-12 +130	A0	7.125	0.014	7.05	0.02	3,3
HD161903	SAO141886	17:48:19.22 -01:48:29.7	+8 +0	A2	7.034	0.014	6.97	0.02	3,3
HD161743	SAO209292	17:48:57.93 -38:07:07.5	+3 -10	B9IV	7.623	0.020	7.67	0.03	2,1
FS147	P230-A	19:01:55.27 +42:29:19.6	-1 +0	A0	9.84	0.02			3,0
GL748	G22-18	19:12:14.60 +02:53:11.1	+1789 -520	M3.5V	6.012	0.020	6.00	0.03	2,2
FS148	S810-A	19:41:23.52 -03:50:56.1	-1 -4	A0	9.46	0.02			4,0
FS149	P338-C	20:00:39.25 +29:58:40.0	+5 -4	B7.5	10.06	0.02			5,0
BS7773	HD193432	20:20:39.82 -12:45:32.7	+16 -15	B9IV			4.86	0.02	0,3
FS150	CMC513807	20:36:08.44 +49:38:23.5	+8 +9	G0	9.91	0.02			4,0
GL811.1	Wolf 896	20:56:46.60 -10:26:54.6	-24 -1110	M2.5V	6.691	0.014	6.72	0.02	3,3
HD201941	SAO126618	21:12:45.32 +02:38:33.9	-28 -20	A2			6.63	0.03	0,3
HD203856	SAO71278	21:23:35.53 +40:01:07.0	+29 +7	A0	6.871	0.013	6.84	0.02	5,3
SAO34401	HD212533	22:23:42.24 +55:12:25.1	+13 -1	F0V	7.735	0.013	7.70	0.02	6,3
BS8541	HD212593	22:24:30.99 +49:28:35.0	-5 -3	B9Iab			4.20	0.02	0,3
FS155	CMC516589	23:49:47.82 +34:13:05.1		K5	9.32	0.02			5,0



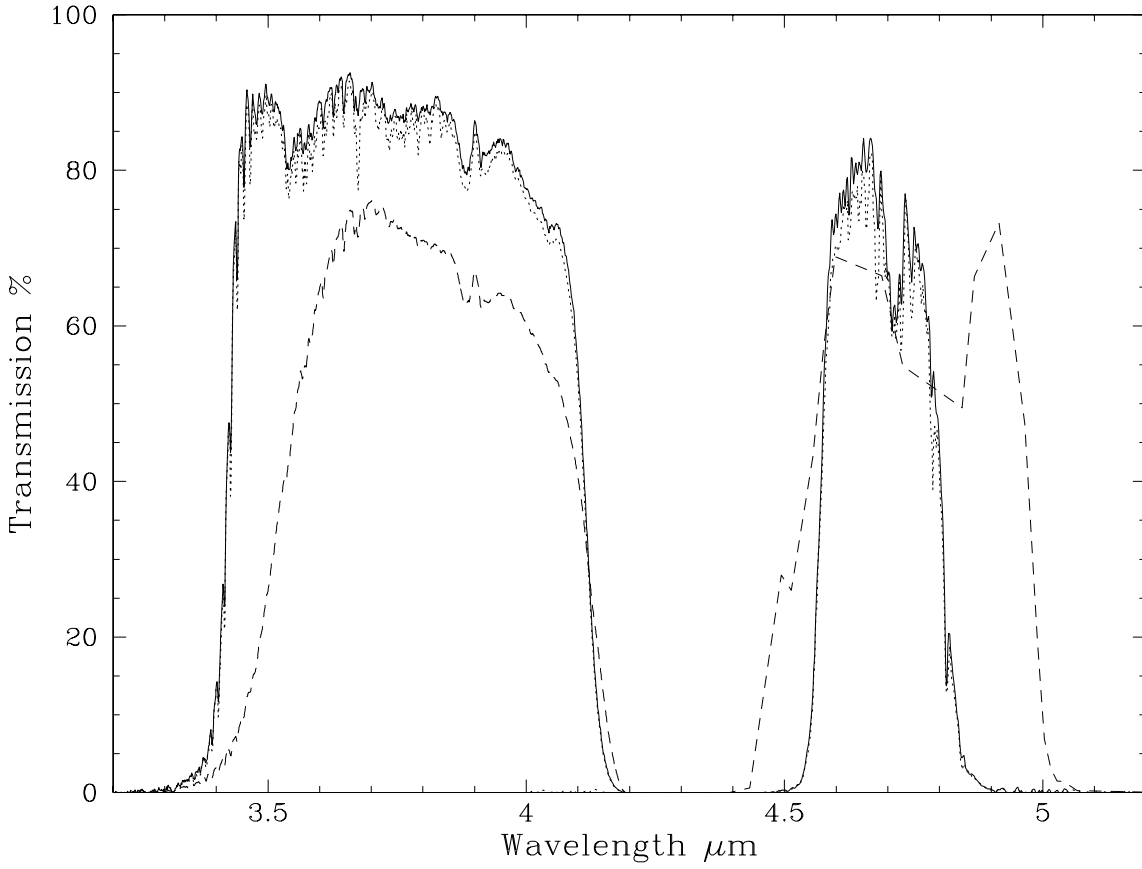


**Figure 1.** Transmission profiles for the current Mauna Kea consortium L' and M' filters for cold, instrument, temperatures, including the effect of absorption by the atmosphere. Solid line is for dry conditions with a precipitable water column of 1.2 mm, and the dotted line for wetter conditions of 3 mm water vapour. Other transmission factors such as detector QE and telescope and instrument optics are effectively flat across the bandpasses and are not included (see discussion in text). The dashed line shows the profile for the previous UKIRT system L' and broadband M filter.

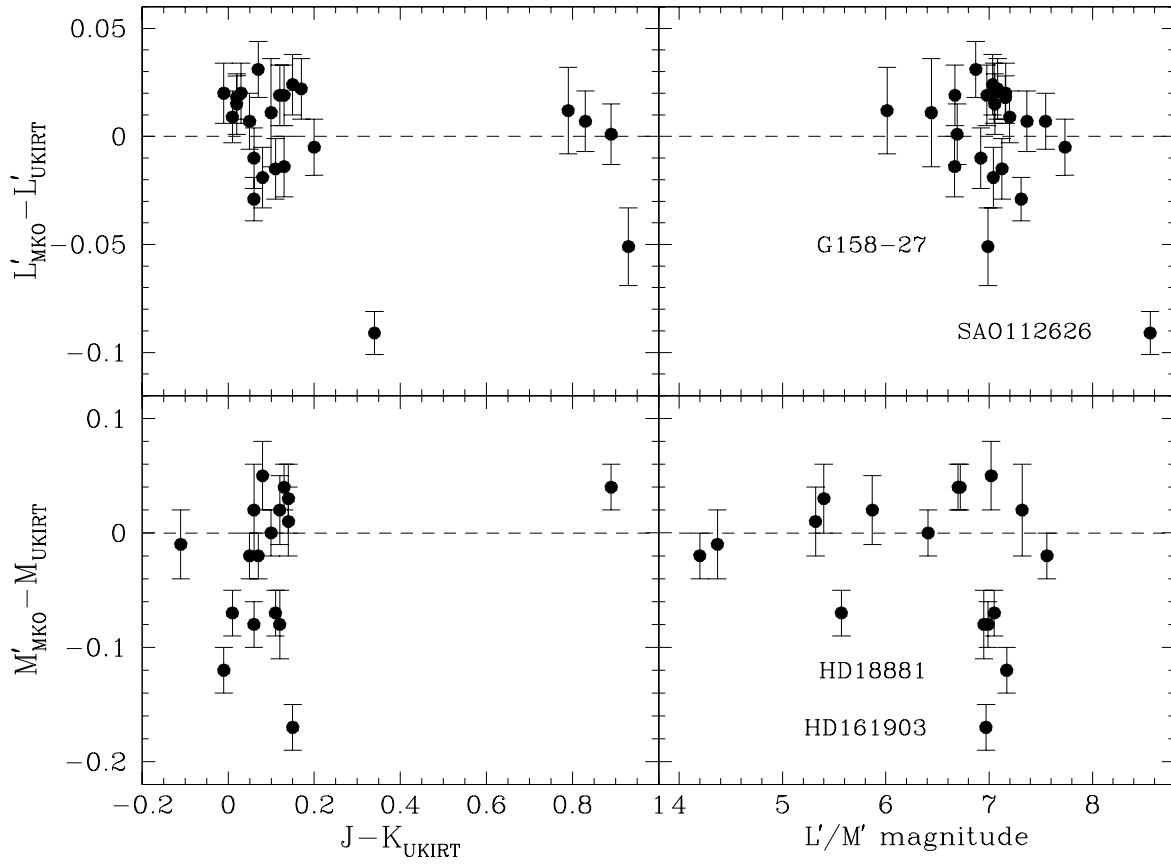


**Figure 2.** Comparison of present results with previous UKIRT system magnitudes, left panel as function of colour, right panel as a function of brightness. See text for discussion.